Performance study of the neutron-TPC*

Meng Huang(黄孟)[1;1)] Yulan Li(李玉兰)[1;2)] Libo Niu(牛莉博)[1] Zhi Deng(邓智)[1]
Xiaolei Cheng(程晓磊)[2] Li He(何力)[1] Hongyan Zhang(章洪燕)[1] Jianqiang Fu(傅楗强)[1]
Yangyang Yan(闫洋洋)[1] Yiming Cai(蔡一鸣)[1] Yuanjing Li(李元景)[1]

[1] Dept. of Engineering Physics, Tsinghua University,
Key Laboratory of Particle & Radiation Imaging (Tsinghua University), Ministry of Education,
Beijing 100084, China
[2] Nuclear Science and Engineering School, North China Electric Power University, Beijing 102206, China

Abstract: Fast neutron spectrometers will play an important role in the future of the nuclear industry and nuclear physics experiments, in tasks such as fast neutron reactor monitoring, thermo-nuclear fusion plasma diagnostics, nuclear reaction cross-section measurement, and special nuclear material detection. Recently, a new fast neutron spectrometer based on a GEM (Gas Electron Multiplier amplification)-TPC (Time Projection Chamber), named the neutron-TPC, has been under development at Tsinghua University. It is designed to have a high energy resolution, high detection efficiency, easy access to the medium material, an outstanding n/γ suppression ratio, and a wide range of applications. This paper presents the design, test, and experimental study of the neutron-TPC. Based on the experimental results, the energy resolution (FWHM) of the neutron-TPC can reach 15.7%, 10.3% and 7.0% with detection efficiency higher than 10^{-5} for 1.2 MeV, 1.81 MeV and 2.5 MeV neutrons respectively.

Keywords: fast neutron spectrometer, time projection chamber, track reconstruction

PACS: 29.40.Cs, 29.40.Gx, 29.30.Hs **DOI:** 10.1088/1674-1137/41/2/026001

1 Introduction

In the future of the nuclear industry and nuclear physics experiments, fast neutron spectrometer are expected to play an important role. They are likely to be used in the fields of fast neutron reactor monitoring [1], thermo-nuclear fusion plasma diagnostics [2–5], nuclear reaction cross-section measurement [6], and special nuclear material detection [7, 8]. However, for traditional fast neutron spectrometers, it is difficult to achieve both high energy resolution and high detection efficiency, or there are special requirements for the spectrometer medium material (such as ^{3}He and ^{6}Li), neutron source, and neutron beam [9–15]. These factors have restricted the application of traditional fast neutron spectrometers. Therefore, a new type of fast neutron spectrometer, with a high energy resolution, a high detection efficiency, easy access to medium material, an outstanding n/γ suppression ratio, and a wide range of applications, is urgently needed.

Recently, a new fast neutron spectrometer based on a GEM-TPC (Gas Electron Multiplier Time Projection Chamber), named the neutron-TPC, has been under development at Tsinghua University [16, 17], trying to solve the difficulties faced by traditional neutron spectrometers (see Fig. 1). Its basic principle is: when the fast neutron beam passes through the collimator and enters into the neutron-TPC, it may collide with the hydrogen nuclei of the working gas and produce recoiled protons; by measuring the recoil angle (θ) and the energy deposition ($E_{\rm p}$) of the recoiled proton, the neutron energy ($E_{\rm n}$) can be derived:

$$E_{\rm n}=\frac{E_{\rm p}}{\cos^2\theta}=E_{\rm p}(1+\tan^2\theta). \quad (1)$$

Compared with traditional fast neutron spectrometers, the neutron-TPC has the following advantages. 1) The working gas acts as the neutron reaction medium, which avoids the energy straggling caused by the use of a solid neutron conversion film. Therefore, compared with the proton recoil telescope [3, 15], the neutron-TPC is expected to achieve a higher energy resolution. 2) The neutron-TPC can have a large reaction depth in the direction of the incident neutron, and the whole readout endcap is the sensitive area for detecting the recoiled protons. Therefore, it is expected to achieve a high detection

Received 27 July 2016, Revised 8 October 2016
* Supported by National Natural Science Foundation of China (11275109)

1) E-mail: hm.max@126.com
2) E-mail: yulanli@mail.tsinghua.edu.cn

efficiency. 3) Since the specific energy loss ($-\mathrm{d}E/\mathrm{d}x$) of photoelectrons is much less than that of protons, gamma rays and neutrons can be distinguished based on the rate of energy loss. As a result, the neutron-TPC can have a high n/γ suppression ratio. 4) By changing the type and pressure of the working gas, or the size of the gas chamber, neutron energy spectra of different energy ranges can be measured.

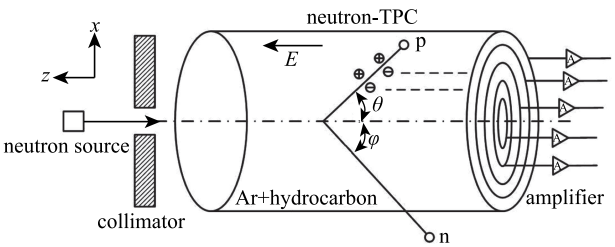

Fig. 1. Working principle diagram of the neutron-TPC.

This paper includes five sections. Section 1 introduces the application background and the working principle of the neutron-TPC; Section 2 presents the design, construction and test of the neutron-TPC; Section 3 focuses on the neutron beam experiment of the neutron-TPC. At last, Section 4 gives a final conclusion.

2 Design, construction and gain calibration

The neutron-TPC was designed based on the TU-TPC [18]. It includes a main chamber (see Fig. 2), electronics, data acquisition and analysis system. The size of the gas chamber of the detector is Φ300 mm×500 mm, allowing the measurement of 1–6 MeV neutrons. Ar-C_2H_6 (50-50) and Ar-CH_4 (70-30) are chosen as the working gases for their good electron drift characteristics and high proportion of hydrogen. A triple-GEM module is employed as the electron multiplier to provide a stable and sufficiently high multiplication factor ($\sim 10^4$), fulfilling the requirement for the signal-noise ratio (>10:1) in the following cosmic ray test and neutron beam experiment [16, 17]. Readout pads are arc-shaped with a width of 2 mm and an arc length of 5 mm, and are distributed around the incident neutron beam. There are 764 readout pads constituting 720 readout channels, due to the channel multiplexing of several pads on the outer rings. Due to the current limit of the number of electronics channels (448 channels), only the part of the readout pads along the 45° direction, named the effective readout pads, are connected to electronics, as shown by the black area in Fig. 2(c). The pre-amplifier ASIC (named CASA-GEM) has a gain factor of 2 mV/fC and a shaping time of 80 ns [19]. The DAQ (Data Acquisition) board has a digitalizing bit of 12 bits and a sampling rate of 25 MHz [20]. The data acquisition program is developed based on LabVIEW software, using the real-time display and data storage functions. The data analysis program is developed based on ROOT software, using the event selection and track reconstruction functions.

Due to the non-uniformity of the GEM detector and following readout electronics, gain calibration must be done before neutron energy measurement. First, the gains of the electronics channels were checked and calibrated using a signal producer. Only 5 of 448 channels were dead, and connected to the edge pads on the readout board, as shown by the red areas in Fig. 2(c). Then, the gain factor of the triple-GEM module was measured using the Cu characteristic X-ray produced by an X-ray machine. The test result shows that the gain performance of the triple-GEM module is excellent. Finally, by measuring and comparing the energy deposition spectra of muon particles on the readout pads, the inconsistency among the channels was calibrated and corrected. In the reconstruction of the energy deposition spectra, only muon events with projected tracks on the x-y plane passing through the center of the readout pads were retained (see Fig. 3). The measurement result shows that, after deducting the gain inconsistency of the electronics channels (relative standard deviation is 6.8%), the gain inconsistency of channels caused by the gain fluctuation of the triple-GEM module is 9.5%.

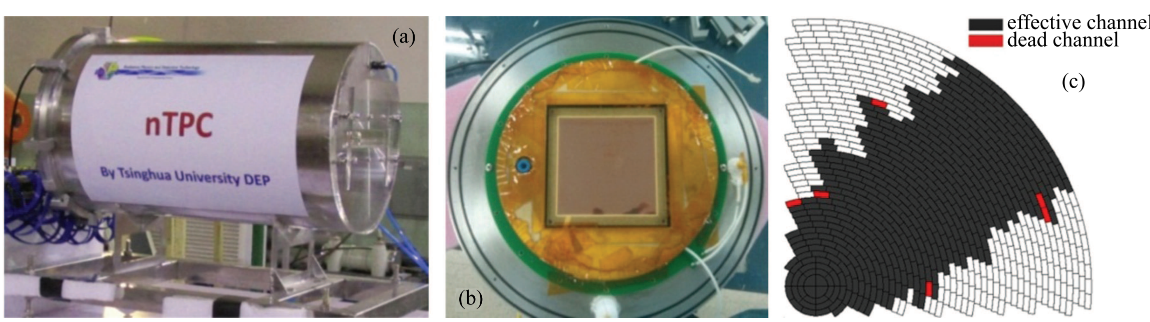

Fig. 2. (color online) Detector appearance (a), readout endcap (b), and readout pads (c).

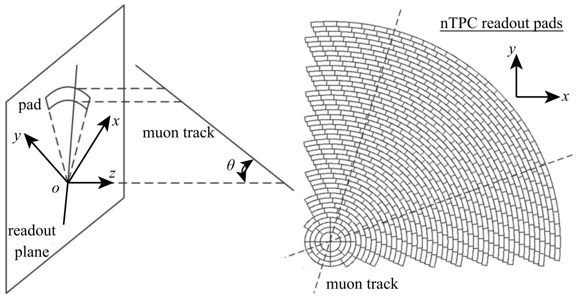

Fig. 3. Correction method for the gain inconsistency of the neutron-TPC channels.

3 Neutron beam experiment

3.1 Experiment setup

The neutron beam experiment was carried out in the Laboratory of Metrology and Calibration Technology, China Institute of Atomic Energy (see Fig. 4). The neutron beams used in the experiment (1.2 MeV, 1.81 MeV and 2.5 MeV) were produced by a small tandem accelerator based on the T(p, n)^{3}He reaction. A polyethylene collimator was used to collimate the neutrons outgoing from the T target. Paraffin shielding was built around the T target to shield the outgoing neutrons in the non-collimation direction. Due to the limitation of the experimental time, only the performance of the neutron-TPC using Ar-CH_4(70-30) as the working gas was studied.

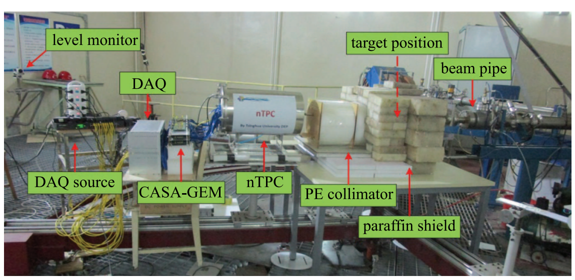

Fig. 4. (color online) Neutron beam experiment site.

3.2 Data analysis

3.2.1 Correction of electron drift velocity

At the beginning of data processing, the analysis result showed that the simulated value of drift velocity of ionized electrons ($v'_{\rm d}$) deviated from the experimental value ($v_{\rm d}$). Based on the analytical formula, one can find the relationship between the reconstructed neutron energy ($E'_{\rm n}$) based on the simulated value of drift velocity of ionized electrons ($v'_{\rm d}$) and the true neutron energy ($E_{\rm n}$):

$$\frac{1}{E'_{\rm n}}=\frac{1}{E_{\rm n}}+\frac{\left(\dfrac{v'_{\rm d}}{v_{\rm d}}\right)^2-1}{E_{\rm n}}\cdot\frac{\tan^2\theta'}{1+\tan^2\theta'}, \tag{2}$$

where θ' is the reconstructed recoil angle of protons based on the simulated value of drift velocity of ionized electrons ($v'_{\rm d}$). By fitting the scatter diagram of $\dfrac{1}{E'_{\rm n}}$ and $\dfrac{\tan^2\theta'}{1+\tan^2\theta'}$ using a straight line, the ratio between the $v_{\rm d}$ and $v'_{\rm d}$ was found and the drift velocity of ionized electrons was corrected.

3.2.2 Elimination of interference signals

In the track finding of the recoiled protons, there may exist some interference signals around the proton track. Through a Hough transformation of the track points on the x-z plane, these interference signals can be discriminated and eliminated (see Fig. 5). The basic method of the Hough transformation is to project the track points from the x-z plane to the ρ-θ plane[21]:

$$\begin{gathered}\rho=\cos\theta\cdot x+\sin\theta\cdot z,\\ -\pi/2<\theta<\pi/2,\ |\rho|\leqslant\sqrt{z_{\max}^2+x_{\max}^2}.\end{gathered} \tag{3}$$

Then, by selecting the intersection point ($\rho_{\max}$, $\theta_{\max}$) crossed by the most curves on the ρ-θ plane and retaining the curves passing through this intersection, the track points of the recoiled proton can be screened out.

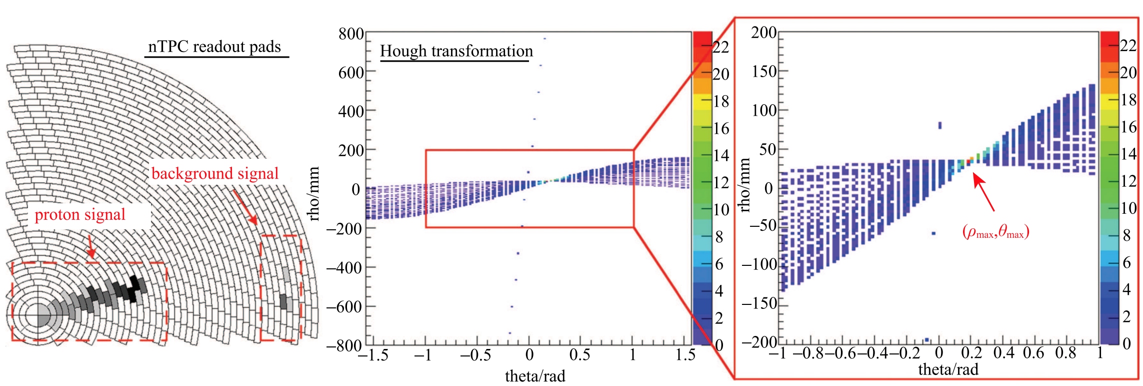

Fig. 5. (color online) Schematic diagram of the Hough transformation.

3.2.3 Discrimination of background events

The experimental data of the neutron-TPC contains a large number of background particles, which interfere with the reconstruction of the neutron spectrum, and need to be discriminated and suppressed. The background particles are mainly divided into four categories according to their sources (see Table 1). 1) The first category is the recoiled protons produced by the scattering neutrons in the experimental hall. These proton events can be excluded by judging whether the initial positions of the particle tracks deviate from the incident neutron beam. 2) The second category includes the recoiled ^{12}C nuclei and ^{40}Ar nuclei produced by the incident neutron beam through elastic collisions between the neutron and the nuclei of the working gas. Because the charge amounts of the recoiled ^{12}C nuclei and the ^{40}Ar nuclei are much larger than the proton, the mean rates of ionization energy loss $\overline{(-\mathrm{d}E/\mathrm{d}x)_{\text{ion}}}$ of these two kinds of particles are much larger than the proton. Therefore, the recoiled ^{12}C nuclei and the ^{40}Ar nuclei can be excluded based on the mean rate of ionization energy loss $\overline{(-\mathrm{d}E/\mathrm{d}x)_{\text{ion}}}$. 3) The third category is the photoelectrons produced by the nuclear reaction associated gamma rays. Because $\overline{(-\mathrm{d}E/\mathrm{d}x)_{\text{ion}}}$ for electrons is much less than for protons, the photoelectrons can also be excluded according to the $\overline{(-\mathrm{d}E/\mathrm{d}x)_{\text{ion}}}$. 4) The fourth category is the recoiled protons produced by the incident neutron beam with part energy deposition collected, named edge protons, including protons hitting the surface of the GEM and protons with projections on the x-y plane exceeding the sensitive area of the readout pads. Because the rate of ionization energy loss at the end of the proton track is far higher than the front track, the $\overline{(-\mathrm{d}E/\mathrm{d}x)_{\text{ion}}}$ of the edge protons is significantly less than the protons with full energy deposition collected. Therefore, the edge protons can be also excluded based on $\overline{(-\mathrm{d}E/\mathrm{d}x)_{\text{ion}}}$.

Figure 6 shows the scatter diagram of the background particles measured with the 2.5 MeV neutron beam. Figure 6(a) shows the track length of the particles and the total charge collected by the readout pads. Figure 6(b) shows the total charge collected by the readout pads and the inclination angle between the particle track and the z-axis. In the figure, the number ① represents the recoiled protons produced by the incident neutron beam with full energy deposition collected, named normal protons; the number ② represents the edge protons; the number ③ represents the recoiled ^{12}C nuclei and ^{40}Ar nuclei; and the number ④ represents the photoelectrons. The recoiled protons produced by the scattering neutrons in the experiment hall have been excluded based on the initial positions of the particle tracks, and are not shown in Fig. 6. As can be seen from the figure, the normal protons with large enough energy (>10 pC) can be easily distinguished from the background particles.

Table 1. Sources and discrimination methods of the background particles.

discrimination method	discrimination method	discrimination method
^{1}H	collision of the scattering neutrons and the working gas	starting position of the particle track
^{12}C, ^{40}Ar	collision of the incident neutrons and the working gas	$\overline{(-\mathrm{d}E/\mathrm{d}x)_{\text{ion}}}$
e^{-}	reaction of the gamma and the working gas	$\overline{(-\mathrm{d}E/\mathrm{d}x)_{\text{ion}}}$
^{1}H	edge protons	$\overline{(-\mathrm{d}E/\mathrm{d}x)_{\text{ion}}}$

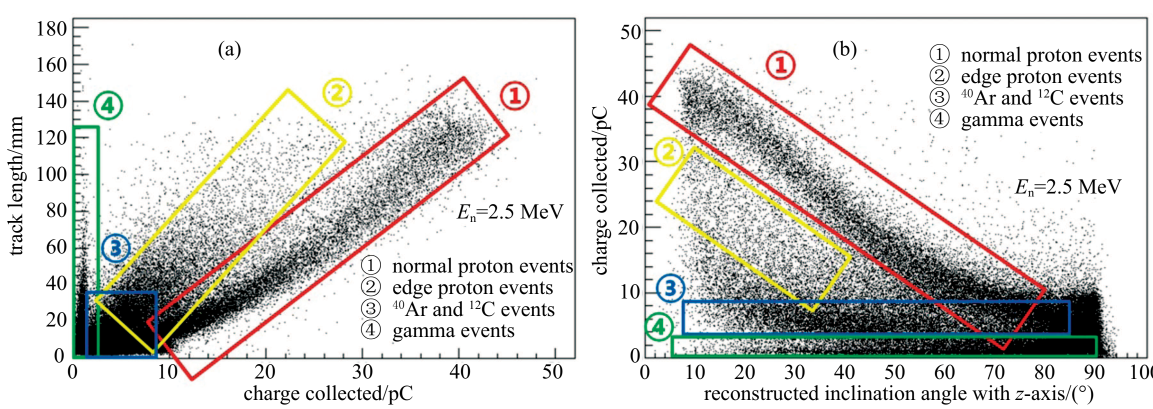

Fig. 6. (color online) Scatter diagram of the background particles measured in the experiment.

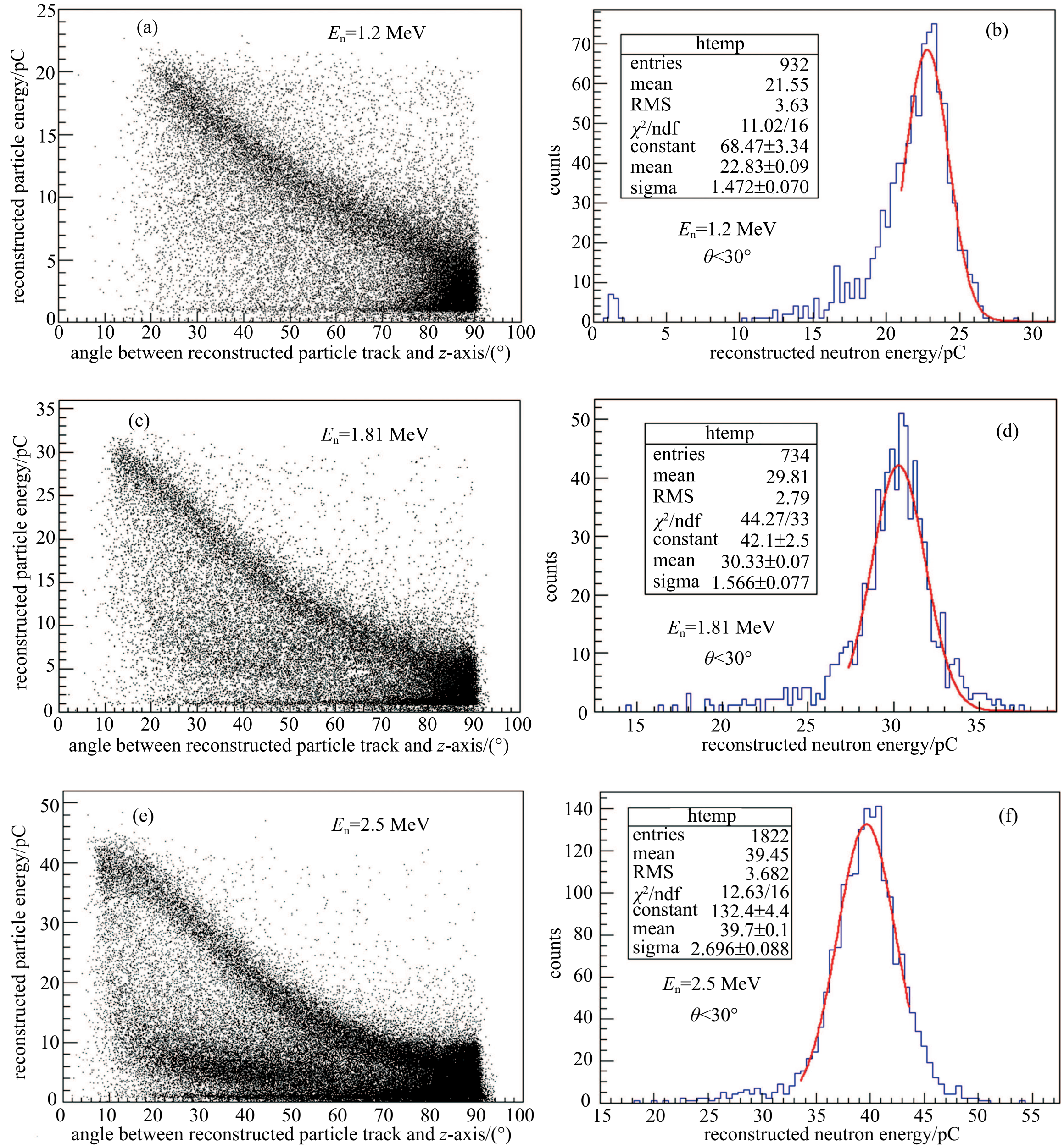

Fig. 7. (color online) Measurement results of 1.2 MeV, 1.81 MeV and 2.5 MeV neutron beams ((a)(c)(e) are scatter plots of reconstructed particle energy and angle between reconstructed particle track and z-axis; (b)(d)(f) are reconstructed neutron spectra).

3.3 Results

In the analysis of the experimental data, the energy information (E_{p}) of the normal protons was obtained by summing the whole energy deposition; the recoil angle (θ) was deduced by fitting the proton tracks on the x-z plane and the y-z plane. By combining the energy and recoil angle of the normal protons, the incident neutron energy (E_{n}) was derived based on Eq. (1). By fitting the reconstructed neutron spectrum using a Gaussian function (see Fig. 7), the charge response of the neutron-TPC to different neutron energies, that is, the energy calibration of the neutron-TPC, was achieved (see Fig. 8). As can be seen from the figure, there is a good linear relationship between the neutron energy and the charge response of the neutron-TPC.

Figure 9 shows the effects of the track fitting ratio (R) (Fig. 9(a)) and the recoil angle cutting (θ_{cut}) (Fig. 9(b)) on the performance of the neutron-TPC in the case of 2.5 MeV neutron beam incidence. The track fitting ratio (R), defined as the ratio of the fitting points (N) and the total number of track points (N_{all}), is used to characterize the fraction of the fitting part in the total track length. As shown in Fig. 9(a), there exists an optimal value of the track fitting ratio (R) to optimize the neutron energy resolution. Meanwhile, the effective neutron detection efficiency will decrease as the track fitting part gets shorter. That is because there exists a threshold for the fitting points (N) in the track fitting process, and tracks with fewer fitting points than the threshold are abandoned. As shown in Fig. 9 (b), the relationship between the neutron energy resolution and the recoil angle cut ($\theta_{\rm cut}$) is monotonically increasing. As the recoil angle cut ($\theta_{\rm cut}$) gets smaller, the neutron energy resolution gets better, while the effective neutron detection efficiency decreases.

Since there still exists certain angle broadening for the neutron beam passing through the collimator, the starting positions of proton tracks may deviate from the axial direction of the neutron beam. As a result, the reconstructed neutron energy from the recoiled proton events with deviated starting positions will deviate from the true value. As the distance between the starting positions of proton tracks and the beam axis gets larger, the deviation between the reconstructed neutron energy and the true value also gets larger. Therefore, by setting the effective area for the starting position of proton track, and screening out recoiled proton events with starting positions far from the beam axis, the energy resolution of the reconstructed neutron spectrum will be improved. Figure 10 shows the effect of the starting position selection of proton tracks on the neutron energy resolution in the case of 2.5 MeV neutron beam incidence. As the figure shows, the energy resolution (FWHM) of the reconstructed neutron spectrum is improved from 11.7% to 9.1%.

By analyzing the influence of the recoil angle cut, the track fitting length, and the starting position of the track on the energy resolution of the neutron-TPC, an optimized neutron energy resolution of the neutron-TPC was achieved, as shown in Table 2. After deducting the energy broadening of the neutron beam, the neutron energy resolution of the neutron-TPC can reach 15.7%, 10.3%, and 7.0% for 1.2 MeV, 1.81 MeV and 2.5 MeV neutrons respectively, with a detection efficiency is higher than 10^{-5}. Because the effective readout pads only cover about 45° quadrant angle, the detection efficiency of the neutron-TPC will be further improved, with the complement of the remaining electronics channels and the expansion of the coverage area of the effective readout pads in the future. The neutron detection efficiency of the neutron-TPC is calculated based on the total neutron yield of the target provided by the Laboratory of Metrology and Calibration Technology, China Institute of Atomic Energy. The calculation formula is as follows:

$$\eta=\frac{N_{\rm spectrum}}{N_{\rm target}\cdot\frac{\Omega\cdot\sigma_\theta}{\sigma}}=\frac{N_{\rm spectrum}\cdot\sigma}{N_{\rm target}\cdot\Omega\cdot\sigma_\theta}, \tag{4}$$

where $N_{\rm spectrum}$ is the counts of the reconstructed neutron spectrum, Ω is the solid angle of the effective area of starting position of recoiled proton tracks relative to the accelerator target, σ_θ is the differential cross section of the T(p, n)^{3}He nuclear reaction, and σ is the total cross section of the T(p, n)^{3}He nuclear reaction.

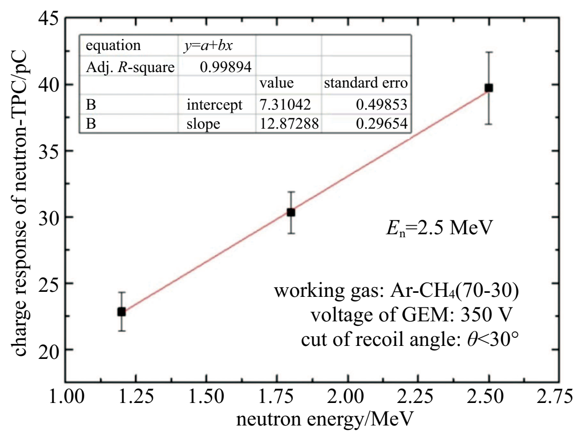

Fig. 8. (color online) Energy calibration of the neutron-TPC.

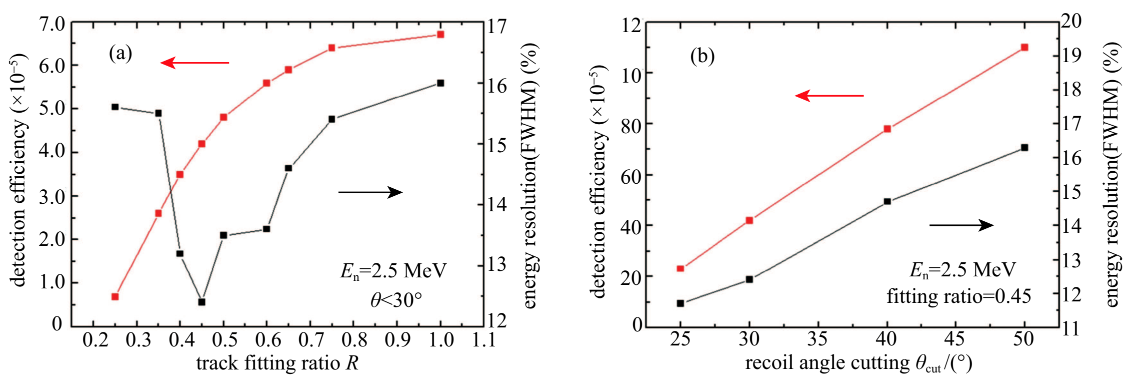

Fig. 9. (color online) Effects of the track fitting ratio (R) and the recoil angle cutting ($\theta_{\rm cut}$) on the performance of the neutron-TPC.

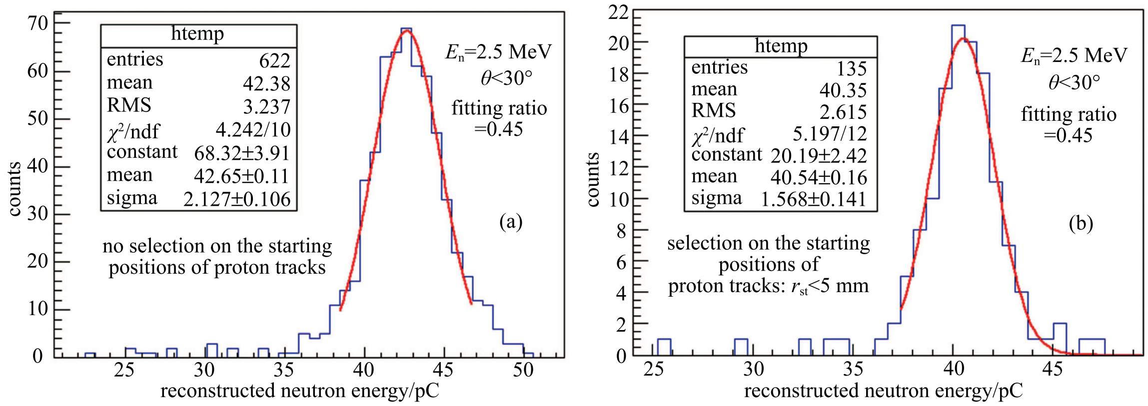

Fig. 10. (color online) Effect of the starting position selection of proton tracks on the neutron energy resolution.

Table 2. Optimized results of the neutron energy resolution.

neutron energy/MeV	recoil angle cutting/(°)	track fitting part (ratio)	starting position of the particle track	energy resolution (FWHM)(%)	detection efficiency
1.2	30	0–1	r_{st} <10 mm	15.7	$3.6^{+0.4}_{-0.4}\times10^{-4}$
1.81	30	0.1–0.6	r_{st} <5 mm	10.3	$6.4^{+0.9}_{-1.0}\times10^{-5}$
2.5	25	0.1–0.4	r_{st} <5 mm	7.0	$1.5^{+0.2}_{-0.2}\times10^{-5}$

4 Conclusion

This paper presents the design, test, and experimental study of the world's first neutron-TPC. First, it was designed based on the TU-TPC. Second, testing of the neutron-TPC was carried out. In particular, by using the correction method based on the cosmic ray measurement, the gain inconsistency of the channels of the neutron-TPC was corrected. Finally, a neutron beam experiment of the neutron-TPC was done. In the experimental data processing, a series of algorithms were employed to eliminate all kinds of interference and background. Based on the experimental results, the energy resolution (FWHM) of the neutron-TPC can reach 15.7%, 10.3% and 7.0% with a detection efficiency higher than 10^{-5} for 1.2 MeV, 1.81 MeV and 2.5 MeV neutrons respectively.

References

1 M. Osipenko, M. Ripani, G. Ricco et al, Nuclear Instruments and Methods in Physics Research A, **799**: 207-213 (2015)
2 T. Matsumoto, H. Harano, A. Uritani et al, IEEE Nuclear Science Symposium Conference Record, **2**: 715-719 (2004)
3 C. Mori, J. Gotoh, A. Uritani et al, Nuclear Instruments and Methods in Physics Research A, **422**: 75-78 (1999)
4 E. I. Moses, R. N. Boyd, B. A. Remington et al, Physics of Plasmas, **16**: 041006 (2009)
5 V. Y. Glebov, D. D. Meyerhofer, T. C. Sangster et al, Review of Scientific Instruments, **77** (10): 715-722 (2006)
6 C. L. Lan, X. C. Ruan, G. C. Chen et al, Nuclear Instruments and Methods in Physics Research B, **375**: 8-12 (2016)
7 R. C. Runkle, A. Bernstein, P. E. Vanier, Journal of Applied Physics, **108** (11): 111101-111101-21 (2010)
8 R. C. Runkle, Nuclear Instruments and Methods in Physics Research A, **652**: 37-40 (2011)
9 J. Yuan, *Design of an extended range multi-sphere neutron spectrometer*, Master Thesis (Beijing: Institute of Modern Physics, University of Chinese Academy of Sciences, 2014) (in Chinese)
10 T. Elevant, Nuclear Instruments and Methods in Physics Research A, **476**: 485-489 (2002)
11 X. B. Jiang, W. S. Zhang, N. Yang et al, Nuclear Techniques, **32** (4): 281-286 (2009) (in Chinese)
12 S. J. Duan, Nuclear Electronics & Detection Technology, **15** (6): 339-347 (1995) (in Chinese)
13 S. Singkarat, N. S. Garis, G. Grosshög et al, Nuclear Instruments and Methods in Physics Research A, **335**: 248-254 (1993)
14 G. Pichenot, S. Guldbakke, B. Asselineau et al, Nuclear Instruments and Methods in Physics Research A, **476**: 165-169 (2002)
15 T. Matsumoto, H. Harano, A. Uritani et al, IEEE Tran. Nucl. Sci., **52** (6): 2923-2926 (2005)
16 M. Huang, Y. L. Li, Z. Deng et al, IEEE NSS-MIC Conference Records, 146-148 (2012)
17 M. Huang, Y. L. Li, L. B. Niu et al, Chinese Physics C, **39** (8): 086003 (2015)
18 Y. L. Li, *The Design, Construction and Experimental Study of a GEM-TPC Prototype*, Ph. D. Thesis (Beijing: Dept. of Engineering Physics, Tsinghua University, 2007) (in Chinese)
19 L. He, Z. Deng, Y. N. Liu et al, Chinese Physics C, **38** (10): 106101 (2014)
20 X. L. Cheng, J. F. Liu, Q. Yu et al, Chinese Physics C, **39** (11): 116103 (2005)
21 L. B. Niu, Y. L. Li, M. Huang et al, Chinese Physics C, **38** (12): 126201 (2014)